American Mineralogist, Volume 80, pages 765–775, 1995

Incongruent dissolution of REE- and Sr-rich apatite in peraluminous granitic liquids: Differential apatite, monazite, and xenotime solubilities during anatexis

MICHAEL B. WOLF, DAVID LONDON
School of Geology and Geophysics, University of Oklahoma, Norman, Oklahoma 73019, U.S.A.

ABSTRACT

The relative solubilities of monazite (Mnz), xenotime (Xno), and apatite (Ap: REE- and Sr-rich, and REE- and Sr-poor) have been studied in peraluminous granitic liquids in month-long experiments at 750 °C and 200 MPa (P_{H_2O}). In contrast with the high solubility of the apatite (0.7 wt% P_2O_5) in strongly peraluminous liquids, monazite and xenotime have much lower solubilities (<0.05 wt% P_2O_5). In mildly to strongly peraluminous compositions, P_2O_5 in the liquid is 0.03–0.04 wt% at xenotime saturation and 0.02–0.05 wt% at monazite saturation; in keeping with the low P in the glasses, RE_2O_3 contents are below EMP detection thresholds ($\leq$0.08 wt%) for all conditions of experiments (saturation of liquid at equilibrium and local saturation around apatite). Apatite dissolves incongruently, crystallizing REE-rich monazite on its surface (1–4 μm-long grains), resulting in similar low REE contents in liquids. Monazite precipitation occurs along the margins of dissolving apatite crystals, even though the bulk liquid is not monazite-saturated. The abundance of monazite microcrystals increases with the REE content of the apatite and the degree of apatite dissolution. The reaction relationship ($Ap + Liq_1 \rightarrow Mnz + Liq_2$), stemming from differences in relative solubilities (greater than an order of magnitude) between apatite and monazite, results in the dissolution of much smaller amounts of REE into peraluminous liquids than expected by simple evaluation of apatite REE contents. The amount of REE contributed from apatite directly to peraluminous granitic liquid is related to the amount of apatite dissolved by simple mass balance only if the total REE content of the apatite is sufficiently low that monazite saturation in liquid (50–100 ppm RE_2O_3 at 750 °C) is avoided. During dissolution of Sr-rich apatite, the Sr partitions into the liquid, and, at 750 °C and 200 MPa (P_{H_2O}), the diffusion coefficient of Sr in liquid is $\sim 2 \times 10^{-10}$ cm²/s ($R^2 = 0.659$).

The reaction relationships described above may have application to some textural features observed in natural igneous rocks. For example, clusters of monazite microcrystals might be indicators of dissolved apatite; monazite morphology can be used to distinguish the source of its REE and the general petrological process (rock anatexis or magma crystallization) under which the monazite formed. In addition, monazite microcrystals could serve as nucleation sites for other minerals, which might explain their common inclusion in biotite and amphibole within granitoids.

INTRODUCTION

Although found only as accessory minerals in most igneous rocks, the phosphates apatite (Ap), monazite (Mnz), and xenotime (Xno) play an important role in determining the rare-earth element (REE) contents of these rocks, especially those that are high in silica (e.g., Nagasawa, 1970; Henderson, 1980; Fourcade and Allègre, 1981; Miller and Mittlefehldt, 1982; Mittlefehldt and Miller, 1983; Weber et al., 1985; Michael, 1988; Reid, 1990; Yurimoto et al., 1990; Suzuki et al., 1992; Watt and Harley, 1993; Wark and Miller, 1993; Zhao and Cooper, 1993). The intracrystalline diffusivity of certain RE and other elements in apatite has been found to be very slow (Watson and Green, 1981; Watson et al., 1985; Cherniak and Ryerson, 1993), and thus the amount of these elements added to the silicate liquid during anatexis typically is considered to depend only on the solubility of apatite. Solubilities have been determined experimentally for apatite (e.g., Watson, 1979; Watson and Capobianco, 1981; Green and Watson, 1982; Harrison and Watson, 1984; Pichavant et al., 1992; Wolf and London, 1993, 1994b) and for monazite (e.g., Rapp and Watson, 1986; Montel, 1986, 1993; Rapp et al., 1987; Ellison and Hess, 1988), and so the important data needed for trace element modeling involving these accessory minerals appear to be available. However, the complex dissolution of apatite, especially in peraluminous granitic magmas, may alter the final amount of trace elements actually added to the liquid. We present evidence here that apatite dis-

0003–004X/95/0708–0765$02.00

TABLE 1. Compositions of minerals and rock powders

	Apatite (REE-poor; Durango, Mexico)	Apatite*	Sr Apatite (Sr- and REE-rich)	Monazite HVD 103880	Xenotime AMNH C68860
SiO_2	0.40	0.04	0.21	2.64	1.89
Al_2O_3	0.00	—	0.01	0.06	0.00
CaO	54.02	54.05	43.67	0.21	0.04
SrO	0.00	0.06	8.83	0.00	0.00
Na_2O	0.03	0.10	0.45	0.00	0.00
K_2O	0.01	—	0.01	0.01	0.01
P_2O_5	41.20	40.90	38.84	23.62	31.78
Y_2O_3	0.04	0.07	0.00	0.18	39.23
La_2O_3	0.46	0.41	1.77	8.92	0.00
Ce_2O_3	0.53	0.50	2.24	25.88	0.05
Nd_2O_3	0.13	0.15	0.42	14.36	0.15
Sm_2O_3	0.02	0.02	0.10	6.74	0.31
Gd_2O_3	0.00	0.04	0.00	5.36	1.06
Dy_2O_3	0.00	0.02	0.01	0.28	4.58
Er_2O_3	0.00	0.00	0.00	0.00	4.23
Yb_2O_3	0.02	0.01	0.00	0.01	4.31
F	n.a.**	3.53	n.a.	n.a.	n.a.
Total	96.86	99.76	96.57	88.24	87.64

Initial rock powder compositions†

	HG	GASI.1	GASI.4	KNPX
SiO_2	76.41	75.81	74.85	73.27
Al_2O_3	14.08	14.60	15.80	13.59
CaO	b.d.t.	b.d.t.	b.d.t.	b.d.t.
Na_2O	5.42	5.45	5.33	5.22
K_2O	4.09	4.14	4.03	4.30
P_2O_5	n.a.	n.a.	n.a.	3.44
Total	91.65	89.39	91.80	90.30
ASI	1.05	1.09	1.20	1.02

Note: HG and GASI.4 powders are mixtures of natural minerals (fired gibbsite added to GASI.4); KNPX is a synthetic gel made from TEOS, nitrates, and phosphoric acid; n.a. = not analyzed; b.d.t = below detection threshold. Additional rock compositions listed in Wolf and London (1994b). The apatites are relatively homogeneous, with 1 sd < 0.3 wt% for CaO, SrO, and P_2O_5 and < 0.1 wt% for other oxides. One standard deviation for monazite is 1.5 wt% for P_2O_5 and <0.5 for other oxides; for xenotime it is 0.8 wt% for Y_2O_3, 0.5 for P_2O_5, and <0.1 for other oxides.

* Electron and proton microprobe analyses (from Roeder et al., 1987); all other data by EMP, this study.

** F not analyzed by EMP because of F migration problems (see Stormer et al., 1993).

† Renormalized on anhydrous basis, except for totals.

solves incongruently to produce monazite (strongly enriched in REE relative to the apatite) plus REE-poor, P-enriched liquid; the importance of this mechanism increases with greater initial concentrations of REE in the apatite and with peraluminosity of the liquid. This mechanism is caused by differences in relative solubilities between apatite and monazite and results in less REE being dissolved into the liquid than expected by a simple evaluation of the apatite REE content (Wolf and London, 1994a).

Our conclusion could have been deduced by a comparison of the previously published sets of data on apatite and monazite solubility, but a direct connection between the differential solubilities of these phosphates and the resultant REE content of the coexisting liquid is made here for the first time. In fact, apatite breakdown with concomitant monazite precipitation during low-temperature alteration has been documented (Boudreau and McCallum, 1990). Our results stem from a previous series of apatite dissolution experiments that were presented in terms of apatite solubilities and dissolution kinetics (Wolf and London, 1993, 1994b). Having determined that the solubility of apatite in liquid (as measured by the concentration of P_2O_5 in glass) increases by over an order of magnitude from mildly peraluminous (0.05 wt% at 1.13 ASI) to strongly peraluminous compositions (0.60 wt% at 1.29 ASI; muscovite-, mullite-, or corundum-saturated), a logical question was what effect does this enhanced solubility in peraluminous liquids have on the ability of apatite to deliver REE to melt? Are the solubilities of the REE-phosphates, monazite and xenotime, modified in the same way and to the same extent? Previous studies showed that monazite solubility increases with increasing peralkalinity (Montel, 1986, 1993) and decreases with increasing peraluminosity (Rapp et al., 1987). Wolf and London (1994b) noticed that monazite precipitated at the surface of dissolving apatite, and that the number of monazite microcrystals increased with increasing dissolution of the relatively REE-poor Durango apatite. This paper investigates the relationship between REE, apatite, monazite, and silicate liquid from previous experiments in addition to new dissolution experiments using REE- and Sr-rich apatite, monazite, and xenotime in peraluminous granitic liquids.

EXPERIMENTAL METHODS

Table 1 lists the compositions of the apatite, monazite, xenotime, and rock powders used in the experiments described in this paper. Natural apatite from Durango, Mexico, with a homogeneous composition close to $Ca_5(PO_4)_3F$ (with ~1.4 wt% RE_2O_3), was mixed with different P- and Ca-free haplogranitic powders made from nearly eutectic proportions of finely ground natural quartz (Brazil), albite (Brazil), and orthoclase (Switzerland), and varying amounts of activated amorphous Al_2O_3 (obtained by decomposing gibbsite at 400 °C). Initial compositions project slightly to the feldspar side of the 200 MPa, H_2O-saturated, Qz-Ab-Or minimum ($Ab_{45}Or_{26.5}Qz_{28.5}$) (Tuttle and Bowen, 1958); measured values of initial Alumina Saturation Index (ASI) [mole ratio $Al_2O_3/(CaO + Na_2O + K_2O)$] range from 1.05 to 1.20. These experiments are described in detail by Wolf and London (1994b). A Sr- and REE-rich apatite obtained from the U.S. National Museum (USNM no. 136827) was added to the strongly peraluminous granitic powder (GASI.4) to study the effect of apatite REE concentration on monazite crystallization. To constrain better the solubility of monazite (and xenotime) under these conditions, natural samples of these minerals were separately added to both the mildly (HG) and strongly (GASI.4) peraluminous haplogranitic powders in a set of dissolution experiments. An additional set of monazite and xenotime dissolution experiments was conducted with a mildly peraluminous, initially P-rich powder (KNPX) to assess the solubility of these minerals as a function of P content.

In all of these experiments, coarse-grained (0.1–0.4 mm³) blocky phosphate mineral fragments were used. Wolf and London (1994b) showed that as the weight ratio of granitic rock powder (liquid) to apatite decreases, the

TABLE 2. Compositional profiles in glasses away from dissolving Sr- and REE-rich apatite

Distance (μm)	HG-36 (4-weeks, GASI.4 powder)				HG-40 (8-weeks, GASI.4 powder)					
	10	30	49	69	10	27	43	60	77	93
	Traverse 1				**Traverse 1**					
SiO_2	65.33	66.51	67.78	68.84	65.93	66.67	66.67	66.65	67.03	67.36
Al_2O_3	16.49	16.01	15.60	15.31	15.92	16.16	15.94	15.76	15.55	15.60
CaO	0.50	0.42	0.38	0.34	0.44	0.46	0.41	0.47	0.42	0.43
SrO	0.10	0.08	0.07	0.08	0.09	0.10	0.12	0.08	0.10	0.09
Na_2O	3.39	3.47	3.50	3.80	3.95	4.02	3.79	3.77	3.83	3.74
K_2O	3.36	3.50	3.48	3.54	3.41	3.52	3.46	3.44	3.32	3.57
P_2O_5	2.38	1.71	1.17	0.64	1.79	1.75	1.64	1.47	1.33	1.12
La_2O_3	0.02	0.00	0.01	0.01	0.00	0.00	0.00	0.01	0.00	0.00
Ce_2O_3	0.02	0.00	0.00	0.01	0.02	0.00	0.00	0.02	0.04	0.03
Sm_2O_3	0.00	0.00	0.00	0.00	0.00	0.00	0.00	0.00	0.00	0.00
Nd_2O_3	0.00	0.00	0.00	0.04	0.03	0.01	0.00	0.00	0.01	0.00
Gd_2O_3	0.00	0.00	0.00	0.00	0.00	0.00	0.00	0.00	0.00	0.00
Total	91.59	91.70	91.99	92.60	91.59	92.69	92.03	91.66	91.61	91.93
Distance (μm)	10	30	51	71	10	28	46	64	82	100
	Traverse 2				**Traverse 2**					
SiO_2	64.76	65.63	65.91	66.80	67.08	67.81	68.58	68.49	69.09	69.41
Al_2O_3	16.26	16.01	15.96	15.75	16.15	15.96	15.79	15.60	15.36	15.14
CaO	0.46	0.44	0.39	0.36	0.50	0.43	0.37	0.36	0.38	0.38
SrO	0.10	0.08	0.09	0.08	0.11	0.08	0.11	0.10	0.10	0.10
Na_2O	3.22	3.97	3.69	3.86	4.00	3.87	4.15	3.90	3.96	4.02
K_2O	3.44	3.57	3.62	3.44	3.47	3.31	3.45	3.43	3.54	3.41
P_2O_5	2.68	2.38	2.03	1.56	1.70	1.39	1.06	0.76	0.50	0.29
La_2O_3	0.00	0.02	0.00	0.00	0.00	0.01	0.03	0.03	0.00	0.01
Ce_2O_3	0.01	0.00	0.01	0.00	0.03	0.00	0.00	0.02	0.03	0.00
Sm_2O_3	0.00	0.00	0.00	0.00	0.00	0.00	0.00	0.00	0.00	0.00
Nd_2O_3	0.01	0.02	0.00	0.01	0.00	0.00	0.00	0.03	0.00	0.00
Gd_2O_3	0.00	0.00	0.00	0.00	0.00	0.00	0.00	0.00	0.00	0.00
Total	90.94	92.13	91.71	91.86	93.03	92.87	93.54	92.71	92.95	92.75

Note: see Table 1 for HG starting compositions. All experiments performed at 750 °C, 200 MPa.

time to approach equilibrium also decreases (for a given apatite grain size and liquid volume). The powder to mineral ratio in the apatite dissolution experiments was kept relatively high (~10:1) to study the kinetics of monazite crystallization during rapid apatite dissolution. The powder to mineral ratio in the monazite and xenotime dissolution experiments was kept relatively low (~2:1) to ensure that elemental concentrations of dissolved mineral components in the glass are equilibrium values (which are measures of the mineral solubilities).

In all experiments, phosphates, rock powder, and H_2O (in excess of that needed for saturation of liquid) were sealed in 20 × 3 mm Au capsules (with powder mix confined to a 5 × 3 mm portion of the capsule). Durations of the experiments ranged from 2 to 15 weeks. Capsules were held subhorizontally in H_2O-pressurized R-41 cold-seal vessels at 200 MPa. Pressure was measured with a factory-calibrated Heise bourdon tube gauge; fluctuations measured over the course of experiments were ≤ 5 MPa. For all experiments, the experiment temperature of 750 °C was measured by internal Chromel-Alumel thermocouples, with an estimated total error ±10 °C. Oxygen fugacity was not controlled, but the intrinsic f_{O_2} of the R-41 vessels is between the NNO and FMQ buffers (e.g., Huebner, 1971). Experiments were quenched isobarically in a jet of compressed air (5–10 °C/s). Capsules were reweighed after the experiment to ensure that they did not leak.

Chemical analyses were obtained by wavelength-dispersive spectrometry on a Cameca SX-50 electron microprobe (EMP). A low beam current (2 nA) and a large diameter spot (13 μm) were used for major elements to minimize volatilization (especially Na); tests using 1, 5, and 10 s repetitive analyses showed no Na loss for total analysis times up to 2 min, so correction factors have not been applied to the Na_2O values. Analytical conditions for major elements were similar to those used by Wolf and London (1994b). The REE were analyzed with a 20 kV, 20 nA, 10 μm diameter beam (for 60 or 120 s on peaks) and calibrated against the REE-bearing glass standards of Drake and Weill (1972). The PAP correction procedure was used (Pouchou and Pichoir, 1985). Calculated detection thresholds (3σ above mean background, in weight percent) are as follows: ≤ 0.02 for major elements; 0.02 for P_2O_5, SrO, and Y_2O_3; 0.05 for La_2O_3, Nd_2O_3, Dy_2O_3, Er_2O_3, and Yb_2O_3; 0.06 for Ce_2O_3 and Sm_2O_3; and 0.08 for Gd_2O_3.

RESULTS

REE- and Sr-rich apatite dissolution experiments

Table 2 lists two sets of glass analyses from EMP traverses from each of the 4- and 8-week, REE- and Sr-rich apatite dissolution experiments (no. HG-36 and 40). As Wolf and London demonstrated (1993, 1994b), the SiO_2, Al_2O_3, P_2O_5, and CaO data show the strong concentration

TABLE 3. EMP analyses of glasses from dissolution experiments

	Monazite dissolution			Xenotime dissolution		
Sample Powder	SOL-28 (14) HG	SOL-29 (14) GASI.4	SOL-30 (13) KNPX	SOL-31 (8) HG	SOL-32 (8) GASI.4	SOL-33 (8) KNPX
SiO_2	69.03 (0.12)	68.19 (0.11)	67.20 (0.08)	69.88 (0.26)	68.93 (0.07)	67.03 (0.17)
Al_2O_3	13.14 (0.06)	14.75 (0.06)	12.71 (0.04)	13.28 (0.14)	14.54 (0.08)	12.73 (0.03)
CaO	0.09 (0.00)	0.09 (0.00)	0.01 (0.00)	0.03 (0.01)	0.03 (0.00)	0.01 (0.00)
SrO	0.00 (0.00)	0.00 (0.00)	0.00 (0.00)	n.d. (—)	n.d. (—)	n.d. (—)
Na_2O	4.67 (0.03)	4.28 (0.03)	4.44 (0.07)	4.90 (0.07)	4.55 (0.04)	4.77 (0.06)
K_2O	3.67 (0.03)	3.39 (0.02)	3.17 (0.02)	3.50 (0.02)	3.35 (0.04)	3.68 (0.03)
P_2O_5	0.02 (0.00)	0.50 (0.01)	2.69 (0.02)	0.03 (0.00)	0.04 (0.00)	3.27 (0.08)
Y_2O_3	n.d. (—)	n.d. (—)	n.d. (—)	0.00 (0.00)	0.00 (0.00)	0.00 (0.00)
La_2O_3	0.01 (0.00)	0.02 (0.00)	0.03 (0.01)	n.d. (—)	n.d. (—)	n.d. (—)
Ce_2O_3	0.03 (0.01)	0.04 (0.01)	0.05 (0.02)	n.d. (—)	n.d. (—)	n.d. (—)
Nd_2O_3	0.02 (0.01)	0.03 (0.01)	0.05 (0.01)	n.d. (—)	n.d. (—)	n.d. (—)
Sm_2O_3	0.00 (0.00)	0.00 (0.00)	0.00 (0.00)	0.00 (0.00)	0.00 (0.00)	0.00 (0.00)
Gd_2O_3	0.00 (0.00)	0.00 (0.00)	0.00 (0.00)	0.00 (0.00)	0.00 (0.00)	0.00 (0.00)
Dy_2O_3	n.d. (—)	n.d. (—)	n.d. (—)	0.02 (0.01)	0.02 (0.01)	0.01 (0.00)
Er_2O_3	n.d. (—)	n.d. (—)	n.d. (—)	0.01 (0.00)	0.03 (0.01)	0.02 (0.00)
Yb_2O_3	n.d. (—)	n.d. (—)	n.d. (—)	0.03 (0.01)	0.04 (0.01)	0.03 (0.01)
Total	90.69 (0.06)	90.83 (0.11)	90.89 (0.12)	91.69 (0.09)	91.54 (0.08)	91.55 (0.14)
ASI	1.11 (0.00)	1.36 (0.01)	1.12 (0.01)	1.12 (0.01)	1.30 (0.01)	1.07 (0.01)

Note: n.d. = not determined; number of analyses listed in parentheses following sample name; standard deviation of the mean listed in parentheses following weight percent.

gradients that develop during melting of semi-isolated apatite grains into peraluminous granitic liquids; within the dissolution aureole, P and Ca are added from the apatite to the liquid, an aluminophosphate complex forms, driving the uphill diffusion of Al, which raises the Al content, and an $AlPSi_{-1}$ exchange reaction occurs, which lowers the Si content. There are no concentration gradients in either Na_2O or K_2O. REE concentrations in the glasses are at or below the detection threshold (b.d.t.) throughout the glasses. There also are no large gradients in SrO (SrO is ≤ 0.12 wt%), although SrO concentrations in the glasses immediately adjacent to the apatite are slightly elevated relative to the other analyses within the profiles; this small gradient was used to determine an approximate diffusion coefficient for Sr at 750 °C (see below). These SrO concentrations, though small, are 4–6 × the 3σ detection threshold (0.02 wt%); analyses of Sr-absent starting compositions consistently yield SrO contents <0.02 wt% (e.g., Table 3).

In all the apatite dissolution experiments, the abundance of monazite crystals at the apatite-glass interface varies with the degree of apatite dissolution (Fig. 1), which is dependent on the ASI of the liquid and the duration of the experiment. Because of the very small grain size (1–4 μm long), reliable analyses of the monazite microcrystals (i.e., uncontaminated by inclusion of glass within the excitation volume) were not obtainable. However, EMP analyses of monazite plus glass regions are qualitatively useful in assessing the relative concentrations of Sr and REE within the apatite, monazite, and glasses (e.g., 0.00–0.05 wt% SrO; 2.7–12.8 wt% La_2O_3; 3.2–17.7 wt% Ce_2O_3; 0.2–1.2 wt% Sm_2O_3; 0.6–2.0 wt% Nd_2O_3; 0.1–2.0 wt% Gd_2O_3). There is clearly a strong concentration of the REE, but not Sr, in the crystallizing monazite relative to the dissolving apatite (compare with RE_2O_3 and SrO contents of the apatites in Table 1 and the glasses in Table 2). Concentration profiles from the REE- and Sr-rich apatite, through monazite (one analysis), and into the glass from experiment no. HG-36 illustrate these trends (Fig. 2): high P_2O_5 contents in apatite and monazite, high CaO contents in apatite but not monazite, and strong concentration gradients in these elements within the glass (Fig. 2a); high levels of SrO, La_2O_3, and Ce_2O_3 in apatite, very high levels of La_2O_3 and Ce_2O_3 in monazite, but almost no REE (b.d.t.) within the glass (Fig. 2b); and a small amount of SrO within the glass but none in the monazite (Fig. 2c).

Concentration profiles of P_2O_5, CaO, and SrO in glass (Fig. 3) show that, under the experimental conditions of 750 °C and 200 MPa, P diffuses only ~200 μm in 4 weeks, whereas both Ca and Sr diffuse >700 μm. Concentrations of P_2O_5 drop to below detection threshold >200 μm from the apatite, but significant, nonzero CaO and SrO contents persist to the edge of the capsule (initial rock powders are Ca and Sr absent; also note the zero values of SrO in the Table 3 analyses from the Sr-absent glasses produced during monazite dissolution). As noted by Wolf and London (1994b), the flat concentration profile of CaO beyond the P diffusion aureole probably results from a Ca diffusivity an order of magnitude greater than that of P and small capsule dimensions relative to the Ca diffusion length; the CaO gradient flattens after Ca diffuses to the edge of the capsule [10 × 200 μm (length of P diffusion aureole) = 2 mm; the distance to the capsule edge is only ~0.7 mm in this direction]. Diffusion coefficients have been calculated for P, Ca, and Sr from the profiles in Figure 3 by plotting the inverse error function (erf^{-1}) of the concentration ratio vs. a distance-time parameter and then measuring the slope of the resulting line. Diffusion coefficients (*D*, in squared centimeters per second) were obtained by squaring the slope of the lines:

$$\frac{x}{2\sqrt{t}} = \sqrt{D}\,\mathrm{erf}^{-1}\left(1 - \frac{C_{x,t}}{C_0}\right)$$

where x = distance from apatite (cm), t = time (s), $C_{x,t}$ = concentration along profile, and C_0 = concentration in glass nearest apatite (after Harrison and Watson, 1983; also see Wolf and London, 1994b). Lines fitted to these data are shown in Figure 4; the calculated diffusion coefficients are $D_P = 9.3 \times 10^{-12}$ cm²/s ($R^2 = 0.994$), $D_{Ca} = 1.1 \times 10^{-10}$ cm²/s ($R^2 = 0.978$), and $D_{Sr} = 2.0 \times 10^{-10}$ cm²/s ($R^2 = 0.659$). The P and Ca data agree with those determined in the previous dissolution study using REE- and Sr-poor Durango apatite (Wolf and London, 1994b).

Results from monazite and xenotime dissolution experiments

The dissolution of REE-bearing apatite produced an abundance of monazite because of an apparent difference in the solubilities of these two minerals. To compare better the solubility of monazite with the previously obtained apatite data, monazite and xenotime were dissolved to determine solubilities as a function of the ASI of the haplogranite liquid. Figure 5 shows the P_2O_5 values in glass vs. ASI both for monazite and xenotime dissolution. Also shown for comparison is a line fit to 106 data points from equilibrated experiments of apatite dissolution from Wolf and London (1994b). The P_2O_5 values are a measure of the solubility of the phosphate minerals in the silicate liquid (Harrison and Watson, 1984) only if there are no large compositional changes in the liquid resulting from the dissolution process (Wolf and London, 1994b); both the equilibrated apatite data and the monazite and xenotime data satisfy this requirement. It is clear from Figure 5 that monazite and xenotime solubilities are much lower than that of apatite and do not appear to be influenced by the ASI of peraluminous liquids. In mildly to strongly peraluminous liquids, P_2O_5 is 0.03–0.04 wt% at xenotime saturation and 0.02–0.05 wt% at monazite saturation.

Table 3 lists averaged glass analyses from each set of monazite and xenotime dissolution experiments. In keeping with the low P_2O_5 contents of the initially P-free glasses (i.e., low phosphate-mineral solubilities; Fig. 5), Table 3 reveals that the RE_2O_3 contents of the glasses are at or below detection thresholds (d.t. of 0.02–0.08 wt%), indicating that both monazite and xenotime have very low solubilities in peraluminous liquids under these conditions [750 °C, 200 MPa (P_{H_2O})].

Discussion

Apatite-monazite relationships

The main point of this paper is to stress the incongruent breakdown of REE-bearing apatite. We have analyzed the peraluminous glasses for REE contents associated with (1) the reaction of apatite to form monazite and (2) the dissolution of monazite and xenotime. Monazite dissolution is discussed before apatite dissolution and monazite formation because it lays the groundwork for the subsequent discussion.

The results from our monazite dissolution experiments (Table 3 and Fig. 5) support the previous work of Montel

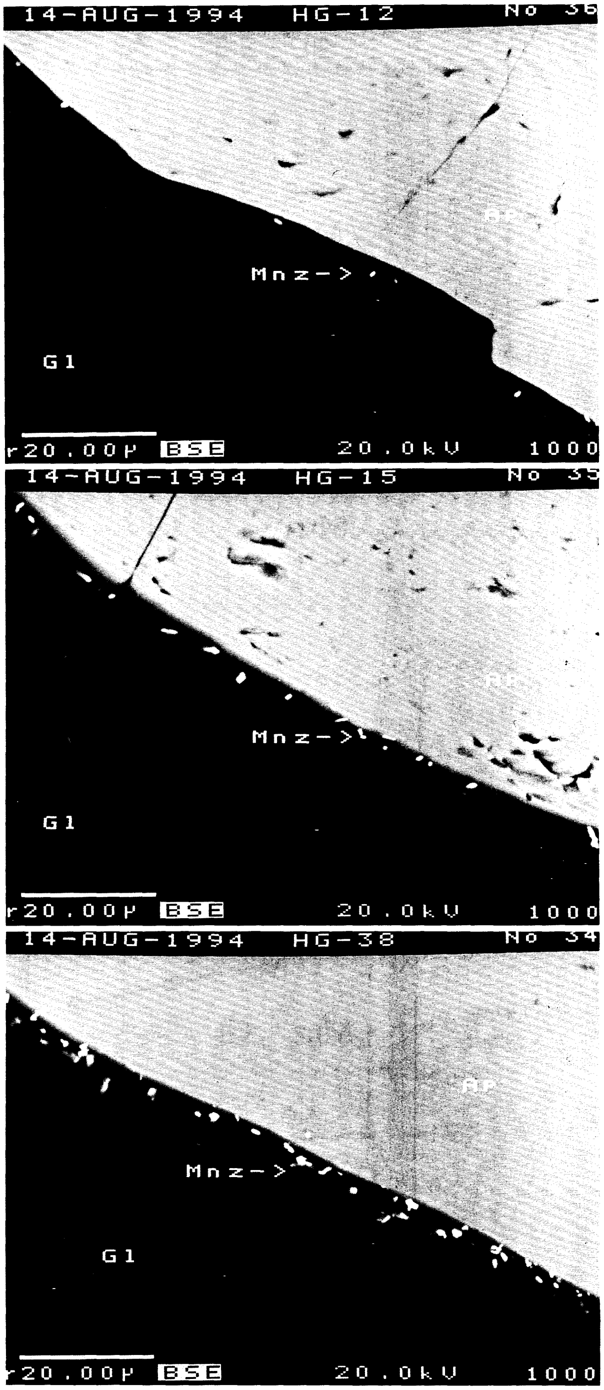

Fig. 1. Back-scattered electron (BSE) images of three Durango apatite dissolution experiments showing the increase in abundance of monazite microcrystals along the apatite-liquid interface as a function of apatite solubility, which increases with increasing Alumina Saturation Index of the liquid [ASI: mole ratio $Al_2O_3/(CaO + Na_2O + K_2O)$]. Ap = apatite; Mnz = monazite; Gl = glass (quenched liquid). Scale bar in micrometers (lower left). All experiments at 750 °C and 200 MPa_{H_2O}. **(top)** No. HG-12, ASI ~1.1, 336 h, GASI.1 powder; **(middle)** no. HG-15, ASI ~1.2, 336 h, GASI.4 powder; **(bottom)** no. HG-38, ASI ~1.3, 694 h, GASI.4 powder plus additional Al_2O_3 (see Table 1 for initial rock powder compositions).

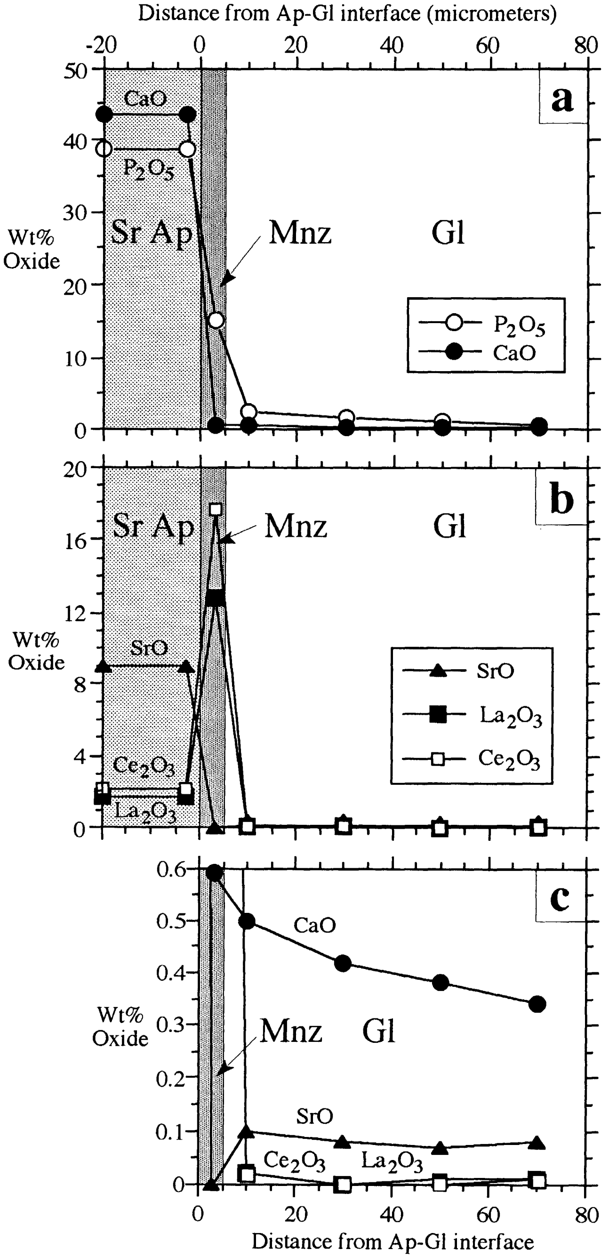

Fig. 2. Concentration profiles from the initial Sr- and REE-rich apatite through a newly crystallized monazite microcrystal at the apatite-glass interface and 70 μm into the glass (no. HG-36, 750 °C, 200 MPa$_{H_2O}$, 672 h, GASI.4 powder, initial ASI ~1.2). (**a**) Profiles of P_2O_5 and CaO (wt%); (**b**) profiles of SrO, La_2O_3, and Ce_2O_3 in the apatite and monazite; (**c**) expanded *y* axis showing profiles of CaO, SrO, La_2O_3, and Ce_2O_3 in the glass.

(1986, 1993) and Rapp and Watson (1986). Figure 6 is a compilation of the monazite solubility data of Montel (1986, 1993), Rapp and Watson (1986), Rapp et al. (1987), and the present study, as determined by total LREE contents in peralkaline to peraluminous granitic liquids. Although there is some discrepancy in the absolute concentrations among data sets, it is clear that increasing the ASI decreases monazite solubility. The compositions used by Rapp et al. (1987) are calcic (0.5–3.0 wt% CaO), which increases monazite solubility (Montel, 1993) and may explain the discrepancies. However, monazite solubility in our experiments is low even with 0.5 wt% CaO in the liquid because of the dissolution of apatite [the starting composition in Rapp and Watson's (1986) work also contains 0.5 wt% CaO]. In addition, the range in SiO_2 for all points is 62–75 wt%, on a hydrous basis, which may explain some of the differences if monazite solubility also depends upon the silica content of the liquid, as does that of apatite (Harrison and Watson, 1984; Wolf and London, 1994b). Ellison and Hess (1988) found that the solubility of $LaPO_4$ (isostructural with monazite) increased not only in peralkaline liquids but also in peraluminous liquids relative to metaluminous ones (K/Al = 1).

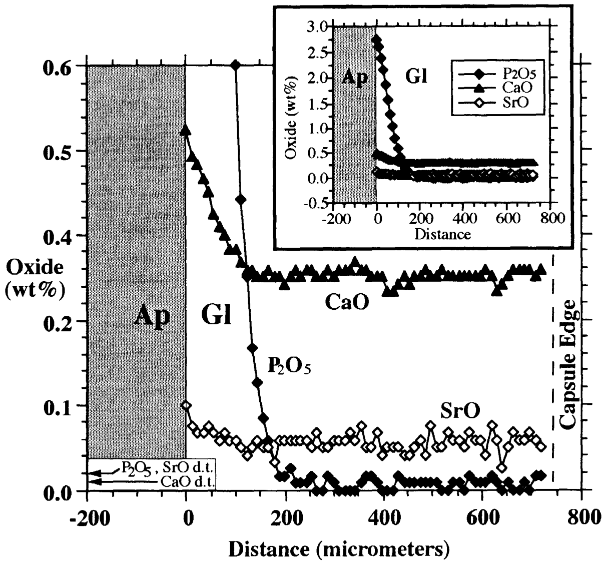

Fig. 3. Profiles of P_2O_5, CaO, and SrO concentrations in glass (no. HG-36; see Fig. 2). Nonzero values of CaO and SrO at >700 μm indicate rapid diffusion relative to P_2O_5. Note P_2O_5, CaO, and SrO detection thresholds (d.t.) of 0.02, 0.01, and 0.02 wt%, respectively. Inset shows full range of P_2O_5 values.

Watson and Capobianco (1981) modeled the effect of residual apatite on the REE contents of felsic liquids by choosing to ignore the effects of other accessory minerals. This simplification may still be warranted when applied to metaluminous liquid compositions, in which apatite solubility is low. Such a simplification clearly does not work with peraluminous compositions because of the direct link between apatite dissolution and monazite crystallization (if the apatite contained abundant Y, Dy, Er, and Yb instead of La, Ce, Nd, and Sm, presumably xenotime would crystallize during apatite dissolution instead of monazite). Most of the REE contained within apatite are not contributed directly to the liquid, so models of anatexis of systems in which peraluminous liquids are produced must account for these differences in phos-

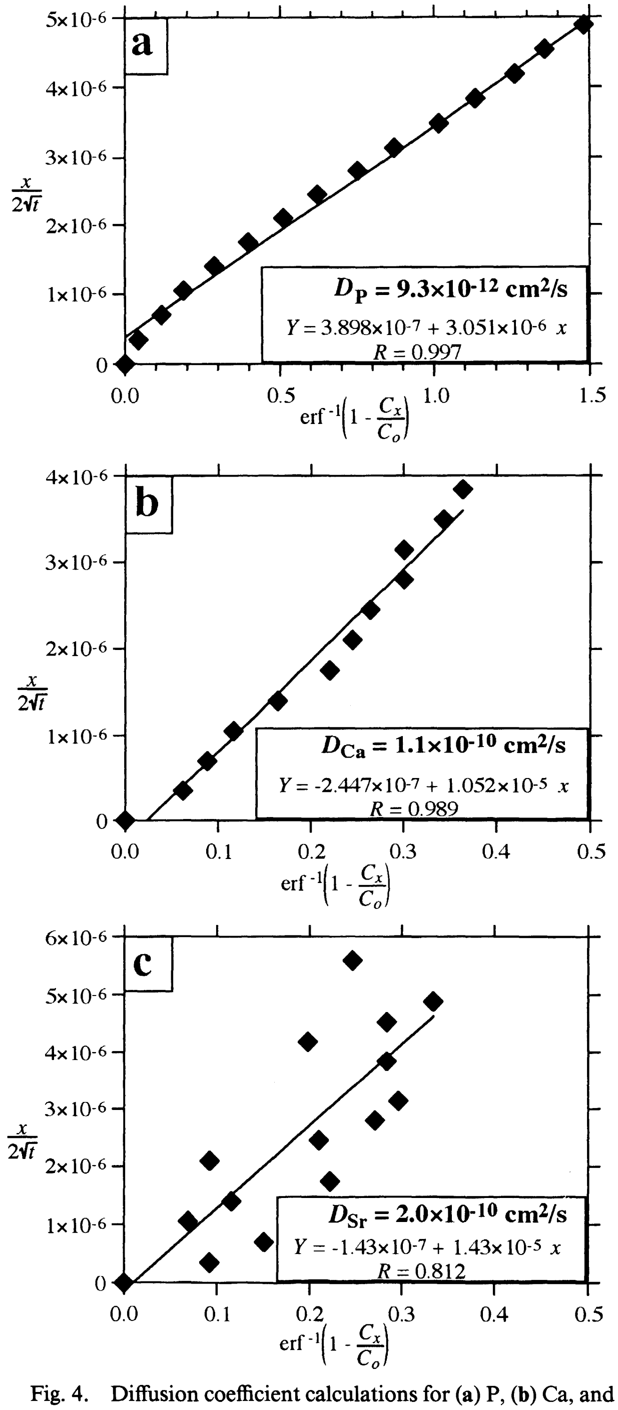

Fig. 4. Diffusion coefficient calculations for (**a**) P, (**b**) Ca, and (**c**) Sr derived from the profiles in Fig. 3. The diffusivities are the slope of the lines squared.

phate mineral solubilities; in other words, monazite and xenotime, not apatite, saturation values must be used to model the contribution of REE from dissolving apatite to peraluminous liquid during anatexis. Apatite contributes only 50–100 ppm RE_2O_3 directly to the liquid; total REE in excess of 50–100 ppm precipitates as monazite or xenotime (on the basis of monazite saturation values of 50–100 ppm RE_2O_3 at 750 °C: Miller and Mittlefehldt, 1982; Rapp and Watson, 1986; Montel, 1993). The total abundance, not the actual composition, of REE dissolved in liquid determines monazite solubility, although the activity of $REPO_4$ is lowered significantly by incorporation of Th and U into the monazite structure (Montel, 1993). It should be noted that liquid compositions derived from metagraywacke, metapelite, and even amphibolite anatexis can be peraluminous and often strongly so (e.g., Vielzeuf and Holloway, 1988; Patiño Douce and Johnston, 1991; Icenhower and London, 1993; Wolf and Wyllie, 1994; Patiño Douce and Beard, 1995), so this mechanism is pertinent to models of partial melting of a wide range of rock types.

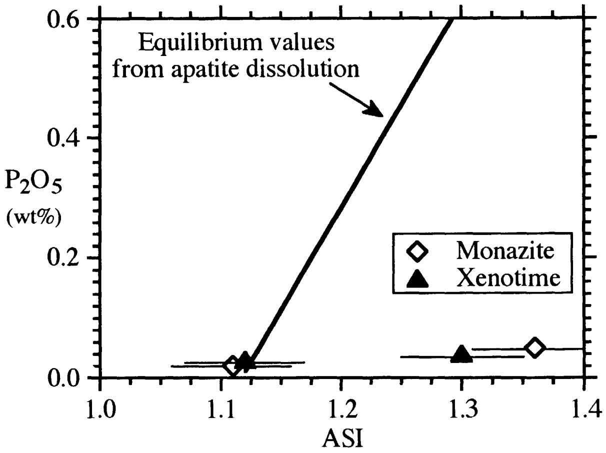

Fig. 5. Monazite and xenotime solubilities (measured as P_2O_5 in the glasses; Table 3) plotted against the Alumina Saturation Index (ASI); 750 °C, 200 MPa_{H_2O}. The line is a fit to the values of apatite solubility determined from equilibrated experiments (from Wolf and London, 1994b).

The generation of natural, strongly peraluminous granitic liquids can occur at temperatures near that of our experiments (750 °C) (e.g., Bea et al., 1994). It may be possible to discern the source of P and REE in these anatectic liquids by comparing their relative abundances. In apatite-bearing source rocks of peraluminous liquids, apatite dissolution will add P to the liquid. Because of the very low solubility of monazite and xenotime under these conditions, most of the REE present in the dissolving apatite will form REE-rich phosphates and will not be added to the liquid (only $\leq$0.05 wt% RE_2O_3 added to the liquid through the incongruent dissolution of apatite; Table 2); however, most of the P will be added to the liquid (not retained in the precipitating monazite), so that the concentration of P_2O_5 will be greater than that of RE_2O_3. At 750 °C, the low REE contents of the liquids are buffered by P_2O_5 values >0.05 wt% (P_2O_5 in excess of 0.05 wt%, e.g., derived from apatite, will complex with available REE in liquid to form monazite). Figure 5 and Table 3 show that the 750 °C equilibrium saturation value of P_2O_5 derived from the congruent dissolution of monazite

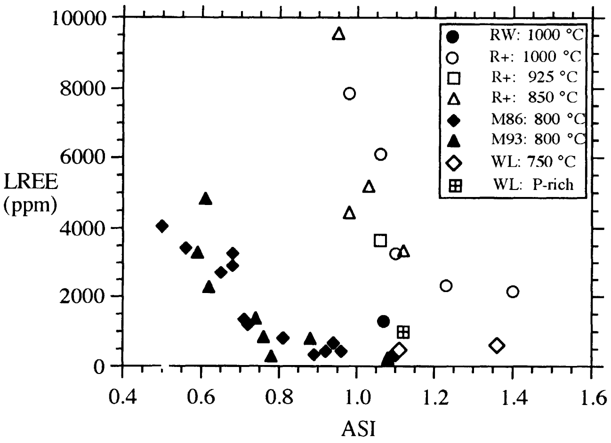

Fig. 6. Experimental monazite solubility data, as determined by total LREE content of the granitic liquids (independent of specific LREE composition), plotted against the Alumina Saturation Index (ASI values < 1 are peralkaline, > 1 are peraluminous). Data are from Rapp and Watson (1986) = RW; Rapp et al. (1987) = R+; Montel (1986) = M86; Montel (1993) = M93; and this study = WL; P-rich sample initially contained 2.7 wt% P_2O_5 (no. SOL-30; Table 3).

and xenotime is ~0.05 wt% P_2O_5; total REE concentrations in monazite- or xenotime-saturated peraluminous liquids also are close to this value (P and REE are approximately stoichiometrically balanced). At higher temperatures, more REE can be dissolved into liquid as the solubility of monazite increases (Rapp and Watson, 1986; Montel, 1993). Rare earth element concentrations equal to that of P imply that monazite or xenotime, not apatite, was the source of REE and P, or that subsequent fractional crystallization of a REE-poor phosphate occurred (however, note that at 750 °C, the mean $D_{\mathrm{REE}}^{\mathrm{Ap/Liq}}$ is ~100, extrapolated from data of Watson and Green, 1981, so that even in monazite-saturated liquids with 100 ppm REE, if apatite were to crystallize, it could contain ~1 wt% total REE).

P, Al, and REE affinities in peraluminous liquids

We have determined that under certain circumstances during rapid breakdown of apatite into peraluminous liquids, the P from the apatite complexes with excess Al from the liquid in a 1:1 cation ratio, possibly as $AlPO_4$ species (Wolf and London, 1994b). Thus, P has an apparent affinity for Al (see also Mysen et al., 1981; Gan and Hess, 1992), which enhances the dissolution of apatite in more aluminous liquids (Pichavant et al., 1987; Montel et al., 1989; London et al., 1990; London, 1992). The data from the current REE- and Sr-rich apatite dissolution experiments substantiate this effect. In contrast, the breakdown of monazite or xenotime is not enhanced by increasing peraluminosity (Fig. 5). Therefore, it appears that the P derived from monazite does not form aluminophosphate species in liquid but remains associated with (i.e., has a stronger affinity for) the REE derived from the dissolving monazite or xenotime. However, Ellison and Hess (1988) found that $LaPO_4$ solubility was greater in peraluminous liquids than in metaluminous ones, which implies that aluminophosphate complexes formed in the liquid; they also noted, though, that P-La interactions appeared to be energetically favorable, especially in calcic liquid compositions. Ryerson and Hess (1978) proposed a P-REE association to explain REE partitioning into the P-rich liquid of a coexisting immiscible pair. The process might be described by a reaction similar to those proposed by Gan and Hess (1992) and Gwinn and Hess (1993): M-O-M + 2(Al-O-P) = 2 M-O-P + Al-O-Al, in which M = metal cation; when M = Ca, this reaction is displaced (in liquid) to the left, and when M = REE, this reaction is displaced to the right. The experimental data are consistent with Rapp and Watson's (1986) proposal that P provides charge compensation for REE during diffusion. Montel (1993) suggested a dissolution mechanism such as $\mathrm{REPO}_4^{\mathrm{Mnz}} \rightarrow \mathrm{REPO}_4^{\mathrm{Liq}}$, in which (1) the REE and P remain associated with each other in the liquid following dissolution, and (2) the solubility of monazite is independent of P activity. Our one result from an experiment in which monazite solubility increased only marginally in a P-rich liquid supports this suggestion (Fig. 6; Table 3, note the similar result from the xenotime dissolution data).

Monazite microtextures after anatexis

Figure 1 shows the texture that develops during the incongruent breakdown of apatite in peraluminous liquids. Microcrystals of monazite precipitate along the apatite-liquid interface, with the density of nucleation increasing with increasing peraluminosity (ASI > 1) and extent of reaction. The microcrystals do not appear to grow much larger subsequent to nucleation, although significant growth could occur in the crystals without detection because of their small size. It is possible that with continued monazite microcrystal growth on the apatite crystal surface, the apatite (especially a REE-rich one) may become encrusted or armored with monazite, which may inhibit further dissolution. However, complete dissolution of an apatite with >100 ppm total REE would leave behind a cluster of monazite or xenotime microcrystals or both. This cluster could define the former presence of the original apatite crystal; monazite clusters in Figure 7 appear to mark the former presence of thin fragments of apatite. If surface tension forces were great enough, the microcrystals could be drawn inward with the retreating apatite-liquid interface, as the apatite dissolves, and could coalesce into a single composite crystal; such a crystal would record any REE heterogeneities in the initial apatite (or the previous liquid from which the apatite crystallized) as a complex, asymmetric zoning pattern within the composite monazite or xenotime (e.g., Jolliff et al., 1989; Wark and Miller, 1993).

Whether or not the monazite microcrystal clusters contract with apatite dissolution, the clusters or even individual microcrystals may serve as excellent sites for subsequent nucleation and growth of other minerals during crystallization and could lead to the formation

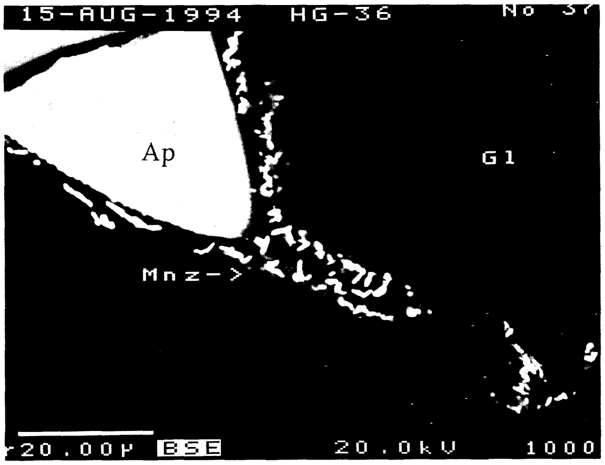

Fig. 7. A back-scattered electron image of the Sr- and REE-rich apatite dissolution experiment (no. HG-36) illustrating that the clustering of monazite microcrystals in a magma may record the former presence of a dissolved apatite crystal (in this case, a thin spine of the partially dissolved apatite fragment). Ap = apatite; Mnz = monazite; Gl = glass (quenched liquid). Scale bar in micrometers.

Fig. 8. Compositionally heterogeneous monazite from granulite-grade metapelite, Blue Ridge, North Carolina, with domains that may be indicative of the incongruent breakdown of apatite and concomitant formation of clusters of monazite microcrystals during anatexis. Texture may have been modified during metamorphism. Scale bar is 100 μm. BSE photomicrograph supplied by Calvin F. Miller.

of inclusion-rich minerals (e.g., Harrison and Watson, 1984; Michael, 1988; Bacon, 1989; Montel, 1993; cf. Watson et al., 1989). Homogeneous dispersion of these closely associated microcrystals throughout a magma could be quite difficult in the absence of vigorous convection, turbulent flow, or supersolidus deformation. Heterogeneous distribution of accessory mineral-rich glomerocrysts within a rock (e.g., Hogan et al., 1993) may reflect the uneven distribution of these restitic clusters of microcrystals within the magma and as inherited from the source region.

Monazite crystallized in our experiments because it was locally saturated along the interface between the liquid and dissolving apatite. Though this mechanism results in precipitation of an accessory mineral, it is quite different from mechanisms proposed for accessory mineral crystallization during phenocryst growth, referred to as the snow plow effect (e.g., Green and Watson, 1982; Harrison and Watson, 1984; Bacon, 1989), in that the REE are derived from the dissolving apatite (not the liquid), and the newly formed monazite does not necessarily become included within a growing phenocryst. Note that monazite initially crystallizes because the liquid along the apatite-liquid interface is oversaturated in REE and P, but the bulk liquid is not saturated. Thus, the monazite microcrystals may dissolve if dispersed throughout the monazite-undersaturated bulk liquid and not incorporated as inclusions within other growing phenocryst minerals. The monazite dissolution rate depends on the temperature, composition, and H_2O content of the magma (Rapp and Watson, 1986). Rapp and Watson (1986) have calculated that, at 750 °C, a small monazite crystal (5 μm radius) would dissolve in a wet (6 wt% H_2O) felsic liquid in ~4000 yr but could persist for 10^9 yr in drier liquids (1 wt% H_2O). However, note that these calculations are based on experimental results that yield a slightly higher monazite solubility limit than those found by Montel (1986, 1993) and by us (Fig. 6).

After taking all the above uncertainties into account, it still might be possible to use the presence of monazite or xenotime microcrystal clusters to indicate the former presence of apatite in crustal xenoliths or any other granulite that is suspected to have melted. We have examined two suites of felsic, lower crustal xenoliths from California that appear to have been melted and subsequently rapidly cooled, quenching the liquid to glass (not devitrified). The electron microprobe analyses of devitrified glasses indicate that the melt was nearly metaluminous, and hence we find apatite but little monazite or xenotime, because apatite is relatively insoluble in metaluminous liquids (Fig. 5). In the absence of partial melts trapped as glass, monazite and xenotime microcrystal clusters as we have described here can be reasonably interpreted to indicate that peraluminous melts were generated from residual source rocks that presently contain these phosphates and once contained apatite with over 100 ppm total REE. We anticipate the detection of this textural and mineralogical association in compositionally more appropriate lithologies such as peraluminous granites and migmatitic metasediments and granulites. In fact, a monazite from a migmatitic granulite-grade metapelite, Blue Ridge, North Carolina (C. F. Miller, 1994 personal communication), shows the compositionally heterogeneous domains that may be indicative of the apatite-to-monazite reaction (Fig. 8). Detection of these textures in other rocks that clearly have been melted would further strengthen the connection between observation and process and may allow extension of the model to rocks with questionable histories. However, even if these textures are indicative of a previous episode of anatexis and apatite dissolution in some rocks, this finding would not necessarily mean that the process occurred in all rocks containing these mineralogical relationships. If the process occurs in nature, then the compositional heterogeneity within the monazite crystals even may record compositional heterogeneities that developed as the apatite crystal grew (e.g., Rakovan and Reeder, 1994), although some recrystallization probably would occur during high-temperature retrograde metamorphism.

Furthermore, in some cases, it may be possible to distinguish the provenance of monazite crystals on the basis of their morphology. The presence of relatively large crystals of monazite (> 100 μm?) may record the precipitation of monazite from locally or bulk monazite-saturated liquid during crystallization of the magma. These crystals are relatively easy to detect using petrographic microscopes. The presence of microcrystals of monazite may record the precipitation of monazite from apatite dissolution during anatexis of the source rock in the absence of conglomeration of the microcrystal clusters. These microcrystals would be very difficult to detect using petrographic microscopes but could be discernible through careful back-scattered electron or X-ray imaging (e.g., Michael, 1988; Wark and Miller, 1993; Montel, 1993). Careful geochemical studies in which all REE could not be accounted for in the mechanically separated accessory mineral fractions (e.g., Suzuki et al., 1990) could indicate a mixed-size population of these minerals, possibly stemming from differences in sources, processes of formation, or both. Further studies incorporating geochemical and experimental data on accessory mineral solubilities (e.g., Reid, 1990) are warranted and even could benefit from intensive petrographic work (e.g., by EMP, SEM, or other microanalytical methods).

ACKNOWLEDGMENTS

This research was supported by the NSF EPSCoR program, grant EHR-91089771, as part of collaborative research between the University of Oklahoma and the University of Tulsa on fluid-rock interactions. We thank George Morgan VI for his valuable assistance during EMP analyses and insightful comments; Sorena Sorenson (Smithsonian: NMNH) and John Hanchar for supplying xenolith suites from the Sierra Nevada and Old Woman-Piute batholiths, respectively; Kazuhiro Suzuki for supplying a Naegi granite sample; Calvin Miller for providing Fig. 8; and Calvin Miller and an anonymous reviewer for their comments on the manuscript.

REFERENCES CITED

Bacon, C.R. (1989) Crystallization of accessory phases in magmas by local saturation adjacent to phenocrysts. Geochimica et Cosmochimica Acta, 53, 1055–1066.

Bea, F., Pereira, M.D., Corretgé, L.G., and Fershtater, G.B. (1994) Differentiation of strongly peraluminous, perphosphorous granites: The Pedrobernardo pluton, central Spain. Geochimica et Cosmochimica Acta, 58, 2609–2628.

Boudreau, A.E., and McCallum, I.S. (1990) Low temperature alteration of REE-rich chlorapatite from the Stillwater Complex, Montana. American Mineralogist, 75, 687–693.

Cherniak, D.J., and Ryserson, F.J. (1993) A study of strontium diffusion in apatite using Rutherford backscattering spectroscopy and ion implantation. Geochimica et Cosmochimica Acta, 57, 4653–4662.

Drake, M.J., and Weill, D.F. (1972) New rare earth element standards for electron microprobe analysis. Chemical Geology, 10, 179–181.

Ellison, A.J.G., and Hess, P.C. (1988) Peraluminous and peralkaline effects upon "monazite" solubility in high-silica liquids. Eos, 69, 498.

Fourcade, S., and Allègre, C.J. (1981) Trace element behavior in granite genesis: A case study; the calc-alkaline plutonic association from the Querigut complex (Pyrénées, France). Contributions to Mineralogy and Petrology, 76, 177–195.

Gan, H., and Hess, P.C. (1992) Phosphate speciation in potassium aluminosilicate glasses. American Mineralogist, 77, 495–506.

Green, T.H., and Watson, E.B. (1982) Crystallization of apatite in natural magmas under high pressure, hydrous conditions, with particular reference to 'orogenic' rock series. Contributions to Mineralogy and Petrology, 79, 96–105.

Gwinn, R., and Hess, P.C. (1993) The role of phosphorus in rhyolitic liquids as determined from the homogeneous iron redox equilibrium. Contributions to Mineralogy and Petrology, 113, 424–435.

Harrison, T.M., and Watson, E.B. (1983) Kinetics of zircon dissolution and zirconium diffusion in granitic melts of variable water content. Contributions to Mineralogy and Petrology, 84, 66–72.

——— (1984) The behavior of apatite during crustal anatexis: Equilibrium and kinetic considerations. Geochimica et Cosmochimica Acta, 48, 1468–1477.

Henderson, P. (1980) Rare earth element partition between sphene, apatite and other coexisting minerals at the Kangerdlugssuaq Intrusion, East Greenland. Contributions to Mineralogy and Petrology, 72, 81–85.

Hogan, J.P., Dewers, T., and Gilbert, M.C. (1993) Minor/accessory mineral segregations in the Reformatory granite. Geological Society of America Abstracts with Programs, 25, 14.

Huebner, J.S. (1971) Buffering techniques for hydrostatic systems at elevated pressures. In G.C. Ulmer, Ed., Research techniques for high pressure and high temperature, p. 123–177. Springer, New York.

Icenhower, J.P., and London, D. (1993) Experimental anatexis and trace-element behaviour in the system Qtz-Ab-Mu+Bt+Als at 200 MPa(H_2O). Eos, 74, 343.

Jolliff, B.L., Papike, J.J., and Shearer, C.K. (1989) Inter- and intra-crystal REE variations in apatite from the Bob Ingersoll pegmatite, Black Hills, South Dakota. Geochimica et Cosmochimica Acta, 53, 429–441.

London, D. (1992) Phosphorus in S-type magmas: The P_2O_5 content of feldspars from peraluminous granites, pegmatites, and rhyolites. American Mineralogist, 77, 126–145.

London, D., Cerny, P., Loomis, J.L., and Pan, J.J. (1990) Phosphorus in alkali feldspars of rare-element granitic pegmatites. Canadian Mineralogist, 28, 771–786.

Michael, P.J. (1988) Partition coefficients for rare earth elements in mafic minerals of high silica rhyolites: The importance of accessory mineral inclusions. Geochimica et Cosmochimica Acta, 52, 275–282.

Miller, C.F., and Mittlefehldt, D.W. (1982) Depletion of light rare-earth elements in felsic magmas. Geology, 10, 129–133.

Mittlefehldt, D.W., and Miller, C.F. (1983) Geochemistry of the Sweetwater Wash pluton, California: Implications for "anomalous" trace element behavior during differentiation of felsic magmas. Geochimica et Cosmochimica Acta, 47, 109–124.

Montel, J.M. (1986) Experimental determination of the solubility of Ce-monazite in SiO_2-Al_2O_3-K_2O-Na_2O melts at 800 °C, 2 kbar, under H_2O-saturated conditions. Geology, 14, 659–662.

——— (1993) A model for monazite/melt equilibrium and application to the generation of granitic magmas. Chemical Geology, 110, 127–146.

Montel, J.M., Mouchel, R., and Pichavant, M. (1989) High apatite solubilities in peraluminous melts (abs.). Terra, 8, 71.

Mysen, B.O., Ryerson, F.J., and Virgo, D. (1981) The structural role of phosphorus in silicate melts. American Mineralogist, 66, 106–117.

Nagasawa, H. (1970) Rare earth concentrations in zircons and apatites and their host dacites and granites. Earth and Planetary Science Letters, 9, 359–364.

Patiño Douce, A.E., and Beard, J.S. (1995) Dehydration-melting of biotite gneiss and quartz amphibolite from 3 to 15 kbar. Journal of Petrology, 36(3), in press.

Patiño Douce, A.E., and Johnston, A.D. (1991) Phase equilibria and melt productivity in the pelitic system: Implications for the origin of peraluminous granitoids and aluminous granulites. Contributions to Mineralogy and Petrology, 107, 202–218.

Pichavant, M., et al. (1987) The Macusani glasses, SE Peru: Evidence of chemical fractionation in peraluminous magmas. In B.O. Mysen, Ed., Magmatic processes: Physicochemical principles (special publication no. 1), p. 359–373. Geochemical Society, University Park, Pennsylvania.

Pichavant, M., Montel, J.M., and Richard, L.R. (1992) Apatite solubility in peraluminous liquids: Experimental data and an extension of the Harrison-Watson model. Geochimica et Cosmochimica Acta, 56, 3855–3861.

Pouchou, J.L., and Pichoir, F. (1985) "PAP" (ϕ-ρ-Z) procedure for improved quantitative microanalysis. In J.T. Armstrong, Ed., Microbeam analysis, p. 104–106. San Francisco Press, San Francisco, California.

Rakovan, J., and Reeder, R.J. (1994) Differential incorporation of trace elements and dissymmetrization in apatite: The role of surface structure during growth. American Mineralogist, 79, 892–903.

Rapp, R.P., and Watson, E.B. (1986) Monazite solubility and dissolution kinetics: Implications for the thorium and light rare earth chemistry of felsic magmas. Contributions to Mineralogy and Petrology, 94, 304–316.

Rapp, R.P., Ryerson, F.J., and Miller, C.F. (1987) Experimental evidence bearing on the stability of monazite during crustal anatexis. Geophysical Research Letters, 14, 307–310.

Reid, M.R. (1990) Ionprobe investigation of rare earth element distributions and partial melting of metasedimentary granulites. In D. Vielzeuf and Ph. Vidal, Eds., Granulites and crustal evolution, p. 507–522. Kluwer, the Netherlands.

Roeder, P.L., MacArthur, D., Ma, X.-P., Palmer, G.R., and Mariano, A.N. (1987) Cathodoluminescence and microprobe study of rare-earth elements in apatite. American Mineralogist, 72, 801–811.

Ryerson, F.J., and Hess, P.C. (1978) Implications of liquid-liquid distribution coefficients to mineral-liquid partitioning. Geochimica et Cosmochimica Acta, 42, 921–932.

Stormer, J.C., Pierson, M.L., and Tacker, R.C. (1993) Variation of F and Cl X-ray intensity due to anisotropic diffusion in apatite during electron microprobe analysis. American Mineralogist, 78, 641–648.

Suzuki, K., Adachi, M., and Yamamoto, K. (1990) Possible effects of grain-boundary REE on the REE distribution in felsic melts derived by partial melting. Geochemical Journal, 24, 57–74.

Suzuki, K., Adachi, M., Yamamoto, K., and Nakai, Y. (1992) Intra-grain distribution of REE and crystallization sequence of accessory minerals in the Cretaceous Busetsu Granite at Okazaki, central Japan. Geochemical Journal, 26, 383–394.

Tuttle, O.F., and Bowen, N.L. (1958) Origin of granite in the light of experimental studies in the system $NaAlSi_3O_8$-$KAlSi_3O_8$-SiO_2-H_2O. Geological Society of America Memoir 74, 153 p.

Vielzeuf, D., and Holloway, J.R. (1988) Experimental determination of the fluid-absent melting relations in the pelitic system, consequences for crustal differentiation. Contributions to Mineralogy and Petrology, 98, 257–276.

Wark, D.A., and Miller, C.F. (1993) Accessory mineral behavior during differentiation of a granite suite: Monazite, xenotime and zircon in the Sweetwater Wash pluton, southeastern California, U.S.A. Chemical Geology, 110, 49–67.

Watson, E.B. (1979) Apatite saturation in basic to intermediate magmas. Geophysical Research Letters, 6, 937–940.

Watson, E.B., and Capobianco, C.J. (1981) Phosphorus and the rare earth elements in felsic magmas: An assessment of the role of apatite. Geochimica et Cosmochimica Acta, 45, 2349–2358.

Watson, E.B., and Green, T.H. (1981) Apatite/liquid partition coefficients for the rare earth elements and strontium. Earth and Planetary Science Letters, 56, 405–421.

Watson, E.B., Harrison, T.M., and Ryerson, F.J. (1985) Diffusion of Sm, Sr, and Pb in fluorapatite. Geochimica et Cosmochimica Acta, 49, 1813–1823.

Watson, E.B., Vicenzi, E.P., and Rapp, R.P. (1989) Inclusion/host relations involving accessory minerals in high-grade metamorphic and anatectic rocks. Contributions to Mineralogy and Petrology, 101, 220–231.

Watt, G.R., and Harley, S.L. (1993) Accessory phase controls on the geochemistry of crustal melts and restites produced during water-undersaturated partial melting. Contributions to Mineralogy and Petrology, 114, 550–566.

Weber, C., Barbey, P., Cuney, M., and Martin, H. (1985) Trace element behaviour during migmatization: Evidence for a complex melt-residuum-fluid interaction in the Saint Malo migmatite complex (France). Contributions to Mineralogy and Petrology, 90, 52–62.

Wolf, M.B., and London, D. (1993) Apatite solubility in the peraluminous haplogranite system—not déjà vu all over again. Eos, 74, 341.

——— (1994a) Incongruent melting of REE-rich apatite in peraluminous granitic melts: Differential apatite and monazite solubilities. Eos, 75, 372.

——— (1994b) Apatite dissolution into peraluminous haplogranitic melts: An experimental study of solubilities and mechanisms. Geochimica et Cosmochimica Acta, 58, 4127–4145.

Wolf, M.B., and Wyllie, P.J. (1994) Dehydration-melting of amphibolite at 10 kbar: The effects of temperature and time. Contributions to Mineralogy and Petrology, 115, 369–383.

Yurimoto, H., Duke, E.F., Papike, J.J., and Shearer, C.K. (1990) Are discontinuous chondrite-normalized REE patterns in pegmatitic granite systems the results of monazite fractionation. Geochimica et Cosmochimica Acta, 54, 2141–2145.

Zhao, J.-X., and Cooper, J.A. (1993) Fractionation of monazite in the development of V-shaped REE patterns in leucogranite systems: Evidence from a muscovite leucogranite body in central Australia. Lithos, 30, 23–32.

MANUSCRIPT RECEIVED SEPTEMBER 8, 1994
MANUSCRIPT ACCEPTED MARCH 22, 1995